HHS Public Access

Author manuscript

J Mol Cell Cardiol. Author manuscript; available in PMC 2020 April 01.

Published in final edited form as:

J Mol Cell Cardiol. 2019 April ; 129: 92–104. doi:10.1016/j.yjmcc.2019.01.015.

Pre-existing fibroblasts of epicardial origin are the primary source of pathological fibrosis in cardiac ischemia and aging

Pearl Quijada[1], **Adwiteeya Misra**[1,2], **Lissette S. Velasquez**[1], **Ryan M. Burke**[1], **Janet K. Lighthouse**[1], **Deanne M. Mickelsen**[1], **Ronald A. Dirkx Jr.**[1], and **Eric M. Small**[1,2,3,4,*]

[1]Aab Cardiovascular Research Institute, University of Rochester School of Medicine and Dentistry, Rochester, NY 14642, USA

[2]Department of Biomedical Engineering, University of Rochester School of Medicine and Dentistry, Rochester, NY 14642, USA

[3]Department of Pharmacology and Physiology, University of Rochester School of Medicine and Dentistry, Rochester, NY 14642, USA

[4]Department of Medicine, University of Rochester School of Medicine and Dentistry, Rochester, NY 14642, USA

Abstract

Serum response factor (SRF) and the SRF co-activators myocardin-related transcription factors (MRTFs) are essential for epicardium-derived progenitor cell (EPDC)-mobilization during heart development; however, the impact of developmental EPDC deficiencies on adult cardiac physiology has not been evaluated. Here, we utilize the Wilms Tumor-1 (*Wt1*)-Cre to delete *Mrtf*s or *Srf* in the epicardium, which reduced the number of EPDCs in the adult cardiac interstitium. Deficiencies in *Wt1*-lineage EPDCs prevented the development of cardiac fibrosis and diastolic dysfunction in aged mice. Mice lacking MRTF-SRF in EPDCs also displayed preservation of cardiac function following myocardial infarction partially due to the depletion of *Wt1* lineage-derived cells in the infarct. Interestingly, depletion of *Wt1*-lineage EPDCs allows for the population of the infarct with a *Wt1*-negative cell lineage with a reduced fibrotic profile. Taken together, our study conclusively demonstrates the contribution of EPDCs to both ischemic cardiac remodeling and the development of diastolic dysfunction in old age, and reveals the existence of an alternative *Wt1*-negative source of resident fibroblasts that can populate the infarct.

*Author for Correspondence Eric M. Small, PhD, Aab Cardiovascular Research Institute, University of Rochester School of Medicine and Dentistry, 601 Elmwood Avenue, Box CVRI, Rochester, NY 14642, Tel: (585)276-7706, Fax: (585) 276-9839, eric_small@urmc.rochester.edu.

AUTHOR CONTRIBUTIONS

P.Q. performed laboratory and animal-based experiments, image acquisition, data quantification, and analysis. A.M. performed the chemokine array and analysis, fibrosis data acquisition and analysis. L.S.V and R.A.D. performed animal-based experiments. R.M.B. and J.K.L. performed laboratory-based experiments. D.M.M. performed and analyzed echocardiography data. P.Q. and E.M.S. designed all experiments and wrote the manuscript. E.M.S conceived of and directed the research.

SUPPLEMENTAL INFORMATION

Supplemental Information includes Supplemental Experimental Procedures and References, 3 Supplemental Tables and 7 Supplemental Figures.

Keywords

epicardium; fibrosis; myocardial infarction; aging; genetic lineage tracing

1. INTRODUCTION

Cardiovascular disease is the leading cause of morbidity and mortality in the United States, and is marked by cardiomyocyte death and the accumulation of extracellular matrix (ECM)[1]. ECM deposition is a mechanism that replaces cardiomyocytes lost following a myocardial infarction (MI), during congenital cardiomyopathy, or in aging[2]. However, left unchecked, excessive ECM leads to pathological fibrosis, or a form of scarring that impedes cardiomyocyte contractility and can initiate lethal arrhythmias[1, 2]. The primary source of scar tissue in the heart is the activated resident fibroblast, called a myofibroblast, which has a high proliferative capacity, becomes contractile and migratory, and secretes copious amounts of ECM[3, 4].

It is thought that the majority of cardiac interstitial cells, including cardiac fibroblasts and vascular mural cells, are derived from a mesothelial layer called the epicardium that covers the developing heart[5, 6]. Lineage tracing studies in transgenic mice harboring Wilms tumor 1 (*Wt1*) or *Tcf21*-directed *Cre* recombinase identified a subset of epicardium-derived progenitor cells (EPDCs) that undergo epithelial-to-mesenchymal transition (EMT) during embryonic development and differentiate into the resident fibroblast lineage[7]. In the adult, ischemia and pressure overload induced cardiac remodeling are associated with re-expression of fetal epicardial genes and expansion of the epicardial layer[7–10]. However, newly activated EPDCs do not appear to populate ischemic tissue, indicating pre-existing fibroblasts are primarily responsible for post-MI scar formation[8, 11]. Instead, the reactivated epicardium may be a source of paracrine factors that contribute to post-MI cardiac remodeling[12]. However, the precise role of *Wt1*-lineage EPDCs in ischemic and non-ischemic cardiac fibrosis has not been functionally tested *in vivo*, and it is not clear whether other sources of cardiac fibroblasts may play a role in cardiac repair.

Recently, our group has demonstrated that myocardin-related transcription factors (MRTF-A and MRTF-B) are required for EPDC mobilization, as their deletion in the epicardium negatively affects epicardial integrity and migration of EPDCs[13]. MRTFs are potent transcriptional activators that are retained in the cytoplasm via interactions with globular (G)-actin[14]. Stimuli that lead to filamentous (F)-actin polymerization, such as mechanical tension or activation of TGF-b and Rho signaling pathways, drive the nuclear accumulation of MRTFs and its interactions with serum response factor (SRF)[14]. MRTF-SRF then induce the expression of the motile/contractile gene program that includes EMT, ECM and contractile proteins[15, 16]. Thus, MRTF-SRF signaling is emerging as a central regulator of fibroblast activation and organ fibrosis[17–21].

In this study, we find that developmental deletion of the MRTF-SRF transcriptional axis in the epicardium using *Wt1*-directed *Cre*-recombinase impedes investment of epicardial-derived interstitial cells in the adult heart. With use of fluorescence-based genetic lineage tracing, we observed that the post-MI scar is populated with epicardium-derived

myofibroblasts, a response that is significantly attenuated with *Srf* deletion from the *Wt1*-positive cell lineage. Constitutive deletion of *Mrtfs* or *Srf* from the epicardium leads to improved functional outcome after MI and reductions in left ventricular fibrosis. Decreased fibrosis is partly due to the paucity of WT1-lineage mesenchymal cells in the scar, which is instead populated with an alternative mesenchymal population that is less fibrotic. Interestingly, deletion of *Mrtfs* from EPDCs also attenuates the accumulation of cardiac fibrosis that contributes to diastolic dysfunction in mice of advanced age. Taken together, this study draws attention to a significant transcriptional program that steers epicardium-derived cells towards a pro-fibrotic phenotype in cardiac disease and normal aging and suggests alternative sources of resident fibroblasts may exist that can contribute to cardiac repair.

2. MATERIALS AND METHODS

2.1. Mice

All experiments using animals were approved by the University Committee on Animal Resources at the University of Rochester. $Mrtfa^{-/-}$ and $Mrtfb^{flox/flox}$ mice were previously described[13] and were gifts from Dr. Eric Olson (UT Southwestern, Dallas, TX, USA). The $Srf^{flox/flox}$ mouse was previously described[22] and was a gift from Dr. Joseph Miano (University of Rochester, Rochester, NY, USA). $Rosa^{mTmG/mTmG}$ mouse strain was purchased from Jackson Laboratories (stock number 007576). The $Wt1^{Cre}$BAC mouse line was previously reported[6] and a gift from Dr. Sylvia Evans (UC San Diego, La Jolla, CA, USA). Breeding strategy for SRF and MRTF transgenic mice, myocardial infarction surgery, echocardiography and physiological assessments are described in the supplemental methods.

2.2. Langendorff technique for isolation of cell populations

Fluorescence-activated cell sorting (FACS) was employed to isolate cardiac cells from tissue. Full details of the langendorff technique are defined in the supplemental methods. FACS was performed using an 18-color BD FACS Aria II (BD Biosciences). If RNA isolation was desired after heart digestion, cells were immediately placed in TRIzol™ Reagent (Thermo Fisher Scientific).

2.3. RNA isolation, cDNA synthesis and Real-Time Quantitative Reverse Transcription PCR

RNA was isolated using TRIzol™ Reagent (Thermo Fisher Scientific) according to the manufacturer's instructions. qRT-PCR was performed with cDNA, primers and IQ SYBR Green Supermix (Biorad). Data was analyzed using the ΔΔCT method.

2.4. Immunohistochemistry

Hearts were paraffin-embedded after perfusion with 10% neutral-buffered formalin (Thermo Fisher Scientific). Sections were cut at a cross-section of 5-μm thickness and multiple levels at 250-μm intervals were analyzing to quantify scar area. Quantitation of protein expression, cardiomyocyte hypertrophy and epicardial numbers are described in the supplemental methods.

2.5. 5-Bromo-2'-deoxy-Uridine (BrdU) injections and in vivo labeling

BrdU (Sigma Aldrich) was administered to mice after sham surgery or myocardial injury at a dose of 50mg/kg daily. Detection of BrdU by immunohistochemistry and quantitation of $BrdU^+$ cells are described in the supplemental methods.

2.6. Fibrosis and infarct size measurements

Picro Sirius Red, Masson's Trichrome and Triphenyl Tetrazolium Chloride staining and quantitation were performed according to details provided in the supplemental methods.

2.7 Proteome Profiler Mouse XL Cytokine Array

A membrane-based antibody array was utilized to measure mouse cytokines from sera isolated from WT and $MRTF^{epiDKO}$ mice. The protocol for simultaneous detection of cytokines was completed according to the manufacturer's instructions (R&D Systems) and developed using a Bio Rad Chemidoc Imaging System Touch Screen System (Biorad). Details associated with the cytokine array are described in the supplemental methods.

2.8. Statistical analyses

All data are expressed as mean +/− SEM. Statistical analyses were performed using unpaired Student's t-test when comparing two groups. One-way ANOVA when comparing multiple groups. Non-repeated two-way ANOVA when comparing multiple groups over a time-course. For oneway and two-way ANOVA, a Tukey post-test was used. All data was analyzed using Graph Pad Prism v7.0. A value of $p<0.05$ was considered statistically significant.

3. RESULTS

3.1. Aged-associated diastolic dysfunction is prevented in $MRTF^{epiDKO}$ mice

To evaluate the impact of disrupting stress-dependent MRTF signaling in EPDCs, we evaluated mice harboring *Mrtf* deletions during the course of normal cardiac aging. Here, we employed the $Wt1^{Cre}$ BAC transgenic mouse[6] to recombine floxed *Mrtf-b* alleles in the context of a global *Mrtf-a* deletion to generate the following lines: 1. Wild-type (WT) 2. *Mrtf-a* null ($MRTF^{AKO}$), 3. Epicardialspecific deletion of *Mrtf-b* ($MRTF^{epiBKO}$) and 4. $MRTF^{AKO}$ plus $MRTF^{epiBKO}$ deletion called $MRTF^{epiDKO}$ mice (Figure 1A). Whole heart digestion followed by fluorescence activated cell sorting (FACS) was performed to isolate CMs, $CD31^+$ and $CD31^-$ populations from healthy WT and $MRTF^{epiDKO}$ hearts in order to evaluate *Mrtf* deletion. $CD31^-$ populations displayed enrichment of the fibroblast marker *Tcf21* (Figure S1A) while $CD31^+$ cells were enriched for the endothelial cell (EC) marker *Pecam1* (Figure S1B). As expected, *Mrtf-a* is not expressed in CMs, $CD31^+$ and $CD31^-$ cells isolated from $MRTF^{epiDKO}$ hearts (Figure 1B). *Mrtf-b* expression is preserved in CMs and $CD31^+$ ECs, but is significantly reduced in the non-endothelial $CD31^-$ cell fraction, which consists of fibroblasts and vascular mural cells (Figure 1C). Consistent with the role of *Mrtfs* in promoting the contractile gene program[16], *Acta2* and *Srf* levels (Figure S1C and S1D) were also reduced in cardiac interstitial cells from $MRTF^{epiDKO}$ mice.

Presentation of diastolic dysfunction with preserved systolic function manifests during cardiac aging due to the accumulation of ECM and inefficient cardiomyocyte relaxation, which impedes proper diastolic filling[23]. Serial echocardiography shows that ejection fraction (EF), a measure of systolic function, was not significantly altered in WT or MRTF^{epiDKO} female mice between 10-weeks and 78-weeks of age (Figure 1D and Figure S2A and S2B). In contrast, we observed diastolic functional decline between 52 and 78 weeks of age in WT mice, as assessed by E to E' ratio via tissue doppler echocardiography, while aged MRTF^{epiDKO} mice maintained diastolic function at these timepoints (Figure 1E and Figure S2C and S2D). Consistent with improved diastolic function, 78-week old MRTF^{epiDKO} mice display reduced collagen deposition in the left ventricle as compared to age-matched WT controls (Figure 1F and 1G). Interestingly, we noted that epicardial cells expressing platelet-derived growth factor receptor-α (PDGFRα $^{+}$) were retained on the surface of the heart in aged MRTF^{epiDKO} mice (Figure 1H and 1I), supporting previous observations of deficient EPDC mobilization and interstitial cell investment during development[13]. Of note, PDGFRα and α-smooth muscle actin (α-SMA) distribution was similar in aged WT and MRTF^{epiDKO} hearts (Figure S3A–C). Overall, MRTF^{epiDKO} mice are protected from the development of cardiac fibrosis and diastolic dysfunction with advanced age, which may reflect inefficient EPDC mobilization during development or a reduced capacity of EPDCs to secrete ECM during the normal aging process.

3.2. Preservation of cardiac physiology in MRTF^{epiDKO} hearts after MI

To further evaluate the role of EPDCs in fibrotic remodeling, we next examined the impact of *Mrtf* deletion from the epicardium on EPDC mobilization and cardiac function following ischemic cardiac injury (Figure 2A). Similar to our findings during aging, the total number of epicardial cells on the surface of MRTF^{epiDKO} hearts was increased compared to control hearts, which was driven by either an expansion or retention of the PDGFRα^{+} population (Figure 2B and 2C). Although MRTF^{epiDKO} mice had smaller cardiomyocyte (CM) cross-sectional area (CSA) at baseline (Figure 2D and 2E), WT and MRTF^{epiDKO} mice exhibited similar CM hypertrophy after MI (Figure 2E) and a comparable induction of fetal cardiomyocyte genes after MI (Figure 2F). Interestingly, while MRTF^{epiDKO} mice displayed normal systolic cardiac physiology at baseline (Figure 2G), we found that MRTF^{epiDKO} mice exhibited a preservation of EF following MI relative to WT controls (Figure 2H and Figure S4A and S4B). Additionally, MRTF^{epiDKO} mice are protected from increases in end diastolic volume (EndDV) that develops at 14 days post-MI (Figure 2I and Figure S4A and S4B). MRTF^{epiBKO} mice also show improved cardiac function 14 days after MI compared to WT mice (Figure 2H) and both MRTF^{AKO} and MRTF^{epiBKO} mice are protected from dilation 14 days after MI (Figure 2I). To confirm that expression of *Cre* recombinase in the *Wt1* lineage does not influence cardiac physiology, we subjected *Wt1*^{Cre} mice to MI and determined that EF and EndDV were not significantly different between *Wt1*$^{cre/+}$ and *Wt1*$^{+/+}$ animals at baseline or after MI (Figure S5A and S5B).

3.3. MRTF^{epiDKO} mice are protected from pathological fibrotic remodeling following MI

To evaluate infarct size following acute ischemic injury, we stained hearts with triphenyl tetrazolium chloride (TTC) one day following MI. We found that the infarct size was statistically similar, but trending smaller, in MRTF^{epiDKO} mice compared to WT mice

(Figure 3A and 3B). Next, we employed an antibody array to screen a total of 111 common cytokines from serum isolated from healthy and injured WT and MRTF^{epiDKO} mice 3 days post-MI. In non-injured animals (baseline) 92.8% of cytokines were similarly expressed in WT and MRTF^{epiDKO} serum (Figure 3C). In contrast, 45% of cytokines were differentially expressed in MRTF^{epiDKO} mice following MI based on a cut-off of +/− 30% relative to WT (Figure 3D). Of the downregulated cytokines in MRTF^{epiDKO} serum, we noted factors that were associated with processes such as inflammatory cell recruitment and fibrotic remodeling (Figure 3E). Specifically, we observed a 63.5% reduction in Periostin and 73.2% reduction in the inflammatory factor Interleukin-1 alpha (IL-1α) in MRTF^{epiDKO} serum (Figure 3E and 3F). However, the expression levels of inflammatory genes *Interleukin1-β* (*Il1*b) or *Interleukin-6* (*Il6*) were not significantly different in nonmyocytes isolated from WT and MRTF^{epiDKO} hearts 7 days after MI (Figure S6A) and we observed a similar number of CD45^{+} cells in WT and MRTF^{epiDKO} hearts following 14 days of MI (Figure S6B and S6C).

MRTF-A and -B are potent co-activators of SRF-dependent transcription that promote myofibroblast activation[21]. We next asked whether improved post-MI cardiac function may reflect suppression of fibrotic remodeling. Masson's trichrome staining revealed pronounced scar formation in WT hearts, whereas MRTF^{epiDKO} hearts displayed reduced transmural fibrosis at 14 days post-MI (Figure 4A and 4B). qRT-PCR revealed genes encoding myofibroblast markers and ECM proteins (e.g. *Mrtfb*, *Acta2*, *Fn*, *Col1a1*, and *Col3a1*) were reduced in nonmyocytes isolated from MRTF^{epiDKO} hearts in comparison to WT hearts 7 days after MI (Figure 4C). Of note, we also determined that female MRTF^{epiDKO} mice had a modest but significant improvement in post-MI cardiac physiology based on EF and EndDV measurements (Figure S5C and S5D).

To evaluate the distribution of total fibroblasts and myofibroblasts in the heart we stained heart sections for PDGFRα and αSMA, respectively. Neither PDGFRα or αSMA distribution were different between WT and MRTF^{epiDKO} mice after sham surgery (Figure 4E and Figure S7A and S7B). However, while the percentage of αSMA^{+} cells was not considerably altered in the remote and border zone (BZ) regions of MRTF^{epiDKO} hearts after MI (Figure S7C and S7D), we observed a significant reduction in the area of PDGFRα coverage in the BZ regions of MRTF^{epiDKO} hearts (Figure 4D and 4E), supporting a more restricted fibrotic response in MRTF^{epiDKO} mice. In order to evaluate the relative proliferation rate and accumulation of epicardial cells and interstitial cells after MI, we injected mice with 5-Bromo-2'-deoxy-uridine (BrdU) starting on the day of surgery and continuing for 14 days after MI. WT interstitial cells proliferated appreciably more in the remote and BZ regions as compared to MRTF^{epiDKO} hearts (Figure S7F and S7G and Figure 4D and 4F). Importantly, detection of proliferating PDGFRα^{+} cells in the BZ regions of MRTF^{epiDKO} hearts was reduced when compared to WT hearts (Figure 4D and 4F).

Epicardial activation after MI is associated with pronounced epicardial cell expansion[12]. Total numbers of epicardial cells were significantly increased in the BZ areas of MRTF^{epiDKO} hearts as compared to WT controls (Figure 4D and 4G) and increased compared to sham conditions (Figure 2B and 2C). However, this response was not associated with an alteration in the relative distribution of BrdU^{+}, PDGFRα^{+} and BrdU^{+}/

PDGFRα$^+$ epicardial cells located in BZ regions (Figure 4G and 4H). Notably, the relative distribution of non-labeled sub-epicardial cells were modestly increased in the remote and BZ regions of MRTF^{epiDKO} hearts as compared to WT (Figure S7I and Figure 4H). These data suggest that MRTF deletion leads to an accumulation of EPDCs on the heart surface following MI. Collectively, our data show that MRTF^{epiDKO} mice are protected from ischemic injury by a reduction in fibrotic remodeling leading to an overall maintenance of cardiac function.

3.4. SRF is required for EPDC investment of the adult cardiac interstitium

In order to better evaluate the influence of MRTF-SRF on EPDC investment of the adult cardiac interstitium we performed *R26R^{mTmG}* based lineage tracing in conjunction with deletion of floxed *Srf* alleles (SRF^{epiKO}) using the *Wt1$^{Cre/+}$* BAC transgenic mouse line (Figure 5A). *R26R^{mTmG}* allows for membrane targeting of a two-color fluorescent *Cre*-reporter allele. In the absence of *Cre* recombination tdTomato fluorescence is observed in all cells, whereas *Wt1-Cre* recombinase expressing cells (and cell derivatives) will present cell membrane-localized GFP fluorescence and extinguish tdTomato fluorescence in EPDCs. We confirmed using immunofluorescence that *Wt1* lineage-derived cells from SRF^{epiKO} hearts lack SRF protein, while SRF protein remained high in CM nuclei (Figure 5B). Whole heart digestion and isolation of CMs, *Wt1* lineage-derived cells (GFP$^+$) and non-*Wt1* lineage-derived cells (tdTomato$^+$) by FACS revealed specific loss of *Srf* transcripts in the GFP$^+$ fraction of SRF^{epiKO} mice (Figure 5C and 5D; Figure S11A and S11D), but not in CMs isolated from SRF^{epiKO} adult hearts (Figure 5E). Of note, SRF^{epiKO} mice displayed normal EF between 10 and 52 weeks of age (Figure S9A) and following sham surgery (Figure S9B).

Utilizing immunohistochemical techniques, we observed robust investment of *Wt1^{Cre}* lineage-derived cells in the epicardium and myocardial interstitium of adult SRF wild-type (WT) mice (Figure 5F and 5G). In contrast, adult SRF^{epiKO} mice have significantly fewer GFP$^+$ cells in the cardiac interstitium (Figure 5F and 5G). Although the distribution of total PDGFRα$^+$ mesenchymal cells in WT and SRF^{epiKO} hearts was similar at baseline (Figure 5F and 5H), GFP co-localized extensively with PDGFRα$^+$ cells only in WT mice (Figure 5F and 5H). Instead, we observed an accumulation of GFP$^-$;PDGFRα$^+$ cells in the interstitium of SRF^{epiKO} hearts at baseline (Figure 5F–5H). Consistent with the phenotype observed in sham MRTF^{epiDKO} mice, the total number of epicardial cells and GFP$^+$ epicardial cells were significantly increased on the surface of SRF^{epiKO} hearts (Figure 5I and 5J); however, the proportion of GFP$^+$ alone, PDGFRα$^+$ alone and GFP$^+$/PDGFRα$^+$ cells was not significantly altered between WT and SRF^{epiKO} mice (Figure 5J). Overall, these data indicate that SRF is required for the investment of the cardiac interstitium with *Wt1* lineage-derived PDGFRα$^+$ mesenchymal cells, and that PDGFRα$^+$ cells are derived from a GFP$^-$ source in SRF^{epiKO} mice, which may represent a WT1-independent lineage or possibly WT1-lineage cells that are wild-type due to incomplete Cre-mediated recombination.

3.5. SRF^{epiKO} mice show modest preservation of cardiac function and exaggerated epicardial activation in response to MI

Since investment of the heart with epicardium-derived mesenchymal cells was reduced in sham SRF^{epiKO} mice, we evaluated the functional consequence of epicardium-specific

deletion of *Srf* on post-MI cardiac remodeling (Figure 6A). Cardiac physiology was evaluated by serial echocardiography, revealing a preservation of EF in SRF^{epiKO} mice at 7 and 14 days after MI (Figure 6B and Figure S8A and S8B). Although SRF^{epiKO} mice displayed improved EF in the late stages of cardiac remodeling, improvement in end systolic volume (EndSV) attained statistical significance only at 7 days after MI and normalized thereafter (Figure 6C and Figure S8A and S8B). Improved functional outcome after MI in SRF^{epiKO} mice was accompanied with a small but insignificant reduction in fibrosis 14 days after injury (Figure 6D and 6E). Consistent with findings using $MRTF^{epiDKO}$ mice observed greater numbers of epicardial cells on the surface of the heart in SRF^{epiKO} mice both in the remote and BZ regions, indicating retention of EPDCs on the heart surface, or exaggerated epicardial activation (Figure S9C–S9E and Figure 6F–6H **and as compared to sham conditions in** Figure 5F and 5I). Notably, the number of $PDGFR\alpha^+$ cells stemming from the epicardium was significantly reduced in the epicardial cell layer in SRF^{epiKO} mice resulting in a relative increase in non-labeled epicardial cells (Figure 6H).

3.6. Infarct re-cellularization requires SRF expression in EPDCs.

We next evaluated cellularization of the infarct by *Wt1*-lineage EPDCs. WT hearts exhibited a robust accumulation of GFP^+ and GFP^+/ $PDGFR\alpha^+$ cells in the remote and BZ regions of the infarct following MI (Figure S9F and S9G and Figure 7A–7C). In contrast, we observed considerably fewer GFP^+ and $GFP^+/PDGFR\alpha^+$ cells in the BZ of SRF^{epiKO} hearts, which were instead populated with $GFP^-/PDGFR\alpha^+$ cells emanating from perivascular regions (Figure 7A–7C). In order to examine the possible contribution of hematopoietic system-derived cells within the infarct, we analyzed WT and SRF^{epiKO} hearts by labeling for the pan-hematopoietic marker CD45. We did not observe any significant changes in the contribution of bone marrow derived cells in the infarct regions of SRF^{epiKO} hearts as compared to WT hearts (Figure S10A and S10B). Additionally, we did not observe significant differences in the expression of *Il1β* or *Il6* from GFP^+ or $tdTomato^+$ cells isolated from WT or SRF^{epiKO} hearts (Figure S10C and S10D). Co-localization of GFP with αSMA expression was also similar between WT and SRF^{epiKO} sham conditions (Figure S10E–S10G). Although αSMA^+ area increased after MI (Figure S10E–S10G), which is consistent with previous reports that utilize SMA as an indicator of the myofibroblast phenotype[24], co-localization of $GFP^+/\alpha SMA^+$ in the remote and BZ regions was not significantly different between WT and SRF^{epiKO} mice (Figure S10E and S10G and Figure 7A). We also confirmed that the total number of GFP^+ cells isolated via FACS was less in sham SRF^{epiKO} hearts consistent with our immunohistochemical analysis (Figure S11A–S11C). Additionally, the total numbers as well as the percentage of GFP^+ cells were significantly reduced in SRF^{epiKO} mice after MI (Figure S11D–S11G).

We next compared gene expression in $GFP^+/PDGFR\alpha^+$ (*Wt1*-lineage cardiac fibroblasts or CFs) compared to $tdTomato^+/PDGFR\alpha^+$ (*Wt1* independent CFs) cells isolated from mice subjected to sham surgery and MI (Figure S11A and S11D); importantly, *Pdgfra* expression was enriched in the $PDGFR\alpha^+$ population after sham and MI surgery (Figure S11M and S11N). *Postn* was significantly increased in both the $tdTomato^+$ and GFP^+ CFs after MI compared to sham mice, although GFP^+ CFs expressed significantly more *Postn* than $tdTomato^+$ CFs. Surprisingly, *Postn* mRNA levels are greater in GFP^+ CFs derived from

SRF^{epiKO} mice than those from WT mice (Figure 7D). *Col1a1*, *Col1a2*, and *Col3a1* are also enriched in GFP^{+} CFs isolated from WT mice as compared to tdTomato^{+} CFs, confirming that *Wt1* lineage-derived cells exhibit a robust fibrotic response to cardiac ischemia (Figure 7F–7H). In contrast, *Tcf21* expression, a marker of the quiescent CF, was decreased in tdTomato^{+} and GFP^{+} CFs isolated from WT mice following MI, but not SRF^{epiKO} mice (Figure 7E). Collectively, these data reveal that robust investment of the ischemic zone with pro-fibrotic EPDCs requires the SRF/MRTF transcription factors and that the infarct may be populated by a *Wt1*-independent lineage that is less fibrotic upon disruption of the *Wt1* epicardial lineage.

4. DISCUSSION

Defining the transcriptional programs that regulate myofibroblast activation remains central to the discovery of novel strategies to prevent organ fibrosis due to injury and/or aging. Our group has previously shown that MRTFs control epicardium-derived mural cell investment during development[13]. While the loss of MRTF expression in the embryonic epicardium results in 50% perinatal lethality, likely due to coronary vessel maturation defects, assessment of adult EPDC function in surviving mice after deletion of either MRTFs or SRF has not been previously addressed. Here, we find that although MRTF^{epiDKO} adult mice display profound deficiency in epicardium-derived interstitial cells at baseline, cardiac function is normal. In contrast, SRF and MRTFs drive fibrotic gene expression in epicardium-derived resident fibroblasts during normal aging, and are essential for investment of the infarct with epicardium-derived resident CFs in ischemia.

Consistent with previous reports, we demonstrate that the *Wt1*-lineage yields a majority of PDGFRα^{+} cells during homeostatic conditions and after injury in the adult heart[8, 9, 11]. Normally, the heart will respond to MI by the expansion of epicardium-derived fibroblasts leading to scar formation. In contrast, *Srf* deletion in the *Wt1*-lineage resulted in a compensatory accumulation of PDGFRα^{+} cells from a *Wt1*-negative source. In SRF^{epiKO} hearts, we observed an accumulation of *GFP*-negative fibroblasts with an apparently “less fibrotic” profile **(Schematic shown in** Figure 7I). Based on immunohistochemical and gene expression analyses, the decreased severity of cardiac fibrosis in SRF^{epiKO} mice at least partially stems from the deficiency in WT1-lineage cell numbers and the accumulation of a less-fibrotic alternative population of fibroblasts. Curiously, the expression of *Postn* and several collagens is not reduced in WT1-lineage cells of SRF^{epiKO} mice, as compared to WT. Thus, compensatory molecular mechanisms may exist that promote myofibroblast activation in *Wt1* lineage-derived cells independent of SRF. Additional mechanisms that may be driving myofibroblast activation upon *Srf* deletion include canonical TGF- β1 – Smad signaling and non-canonical TGF-β1 – p38 signaling[25, 26].

While the source of the GFP^{-}/PDGFRα^{+} population that appears following MI in SRF^{epiKO} is not clear, it is possible they are wildtype *Wt1*$^{Cre/+}$ lineage cells following incomplete recombination at the *Srf* and *R26*^{mTmG} loci. Recombination efficiency of Cre driver strains can vary significantly and may be dependent on the activity of transgenic promoters during developmental transitions[27, 28]. Despite the limitations of Cre-based model systems, based on data from our study and others[8, 9], it is likely that an alternative WT1^{-} developmental

source may be responsible for populating the post-MI scar in SRF^{epiKO} mice that is not typically observed in WT conditions, which needs to be tested empirically in future studies. Contributions from this alternative cell population may partially counteract reduced cell numbers, migratory ability, or activity of epicardial-derived mesenchymal cells during cardiac growth and in response to cardiac injury. Although the expression of both Wt1 and Tcf21 is associated with interstitial and epicardial fibrosis in ischemia, Tcf21 is reported as a more unique marker of perivascular fibroblasts in hypertension[10, 29]. It is intriguing to speculate that developmental plasticity exists such that insufficiency of WT1-lineage resident fibroblasts may be compensated for by contributions from another source, such as Tcf21lineage perivascular cells. A similar phenomenon was recently reported, where dysfunction of sinus venosus-derived coronary EC progenitor cells leads to the propagation of endocardium-derived ECs that rebuild the coronary vasculature[30]. Combinatorial genetic recombination strategies would be required to evaluate alternate developmental sources of resident fibroblasts[31]. For example, the *Wt1^{Cre}* mouse line could be used for gene deletion in a background of a FLP lineage reporter system to delineate whether endothelial (Cdh5, Tie2)[32, 33], bone-marrow (Vav, LysM)[34,35], smooth muscle (Myh11)[36], pericyte (Cspg4)[37], or other epicardial and perivascular (Tbx18, Tcf21)[38, 39] lineages are infiltrating the ischemic zones of SRF^{epiKO} hearts.

The epicardium is a highly dynamic structure providing both beneficial and pathological remodeling cues in the heart following injury, and is likely required for cardiac regeneration in zebrafish and neonatal mouse models[40, 41]. In our study, we observed an increased retention of EPDCs on the surface of the heart at baseline and following MI, which contributes to pronounced epicardial thickening observed in *Mrtf* and *Srf* deficient mice. This phenomenon may be advantageous by providing mechanical and/or structural support to prevent infarct expansion. Additionally, the re-activated epicardium has been shown to play cell non-autonomous roles via secretion of paracrine cues to promote cardiomyocyte regeneration and angiogenesis after ischemia in adult mice[12, 42]. In our study, we identified several chemokines that differentially accumulate in the serum of mice exhibiting improved outcomes following MI. Based on our studies, It is possible that cardioprotective or immunomodulatory chemokines originate from the epicardium, and future studies should evaluate epicardial-specific paracrine factors for their ability to enhance cardiac repair following ischemic injury.

A hallmark of cardiac aging is the progressive accumulation of ECM[43]. Remarkably, we show that MRTF^{epiDKO} mice have reduced fibrosis and preserved diastolic function during aging. This data indicates that EPDCs not only contribute to ischemic remodeling, but also to chronic deposition of ECM that ultimately leads to the development of fibrosis and left ventricular stiffening in aging. Our data is in support of recent studies that prevent fibrosis in various cell types by inhibiting the Rho-ROCK/MRTF-SRF signaling axis[17–20, 44] , although recent findings from our lab linking actin-based MRTF transcriptional mechanisms with cardiomyocyte integrity indicate this strategy may be more complicated[45]. Further defining the signaling mechanisms that drive EPDC plasticity in cardiac aging and disease is important for the discovery of novel strategies that block or reverse cardiac fibrosis.

Supplementary Material

Refer to Web version on PubMed Central for supplementary material.

ACKNOWLEDGMENTS

We would like to thank all the members of the Small laboratory for their feedback during the development of this manuscript. We would also like to thank the URMC Flow Cytometry Shared Resource Core for their assistance in performing FACS-based cell isolations. This work is supported by grants: E. Small (NIH R01HL133761, NIH R01HL136179, NIH R01HL120919, and NYSTEM-C32566GG); P. Quijada (NIH T32HL066988 and NIH F32HL134206); R. Burke (NIH T32HL007937 and NIH F32HL136066); and J. Lighthouse (NIH T32HL066988 and AHA 15POST25550114). The laboratory is supported by a Pilot Study Grant from the AabCardiovascular Research Institute at the University of Rochester of Medicine and Dentistry. E. Small is supported in part by a research grant from Novartis Pharmaceuticals.

CONFLICTS OF INTEREST

E.M.S. is a recipient of a research grant from Novartis Pharmaceuticals, which is not related to the current study.

Abbreviations:

MRTF	myocardin-related transcription factors
SRF	serum-response factor
WT1	Wilms Tumor 1
EPDC	epicardium-derived progenitor cell
PDGFRα	platelet-derived growth factor–alpha

References

1. Murtha LA, Schuliga MJ, Mabotuwana NS, Hardy SA, Waters DW, Burgess JK, Knight DA and Boyle AJ. The Processes and Mechanisms of Cardiac and Pulmonary Fibrosis. Front Physiol 2017;8:777. [PubMed: 29075197]
2. Meschiari CA, Ero OK, Pan H, Finkel T and Lindsey ML. The impact of aging on cardiac extracellular matrix. Geroscience 2017;39:7–18. [PubMed: 28299638]
3. Lighthouse JK and Small EM. Transcriptional control of cardiac fibroblast plasticity. J Mol Cell Cardiol 2016;91:52–60. [PubMed: 26721596]
4. Burke RM, Lighthouse JK, Quijada P, Dirkx RA Jr., Rosenberg A, Moravec CS, Alexis JD and Small EM. Small proline-rich protein 2B drives stress-dependent p53 degradation and fibroblast proliferation in heart failure. Proc Natl Acad Sci U S A 2018;115:E3436–E3445. [PubMed: 29581288]
5. Zhou B, von Gise A, Ma Q, Hu YW and Pu WT. Genetic fate mapping demonstrates contribution of epicardium-derived cells to the annulus fibrosis of the mammalian heart. Dev Biol 2010;338:251–61. [PubMed: 20025864]
6. Wessels A, van den Hoff MJ, Adamo RF, Phelps AL, Lockhart MM, Sauls K, Briggs LE, Norris RA, van Wijk B, Perez-Pomares JM, Dettman RW and Burch JB. Epicardially derived fibroblasts preferentially contribute to the parietal leaflets of the atrioventricular valves in the murine heart. Dev Biol 2012;366:111–24. [PubMed: 22546693]
7. von Gise A, Zhou B, Honor LB, Ma Q, Petryk A and Pu WT. WT1 regulates epicardial epithelial to mesenchymal transition through beta-catenin and retinoic acid signaling pathways. Dev Biol 2011;356:421–31. [PubMed: 21663736]

8. Moore-Morris T, Cattaneo P, Guimaraes-Camboa N, Bogomolovas J, Cedenilla M, Banerjee I, Ricote M, Kisseleva T, Zhang L, Gu Y, Dalton ND, Peterson KL, Chen J, Puceat M and Evans SM. Infarct Fibroblasts Do Not Derive From Bone Marrow Lineages. Circ Res 2017.

9. Moore-Morris T, Guimaraes-Camboa N, Banerjee I, Zambon AC, Kisseleva T, Velayoudon A, Stallcup WB, Gu Y, Dalton ND, Cedenilla M, Gomez-Amaro R, Zhou B, Brenner DA, Peterson KL, Chen J and Evans SM. Resident fibroblast lineages mediate pressure overload-induced cardiac fibrosis. J Clin Invest 2014;124:2921–34. [PubMed: 24937432]

10. Braitsch CM, Kanisicak O, van Berlo JH, Molkentin JD and Yutzey KE. Differential expression of embryonic epicardial progenitor markers and localization of cardiac fibrosis in adult ischemic injury and hypertensive heart disease. J Mol Cell Cardiol 2013;65:108–19. [PubMed: 24140724]

11. Ali SR, Ranjbarvaziri S, Talkhabi M, Zhao P, Subat A, Hojjat A, Kamran P, Muller AM, Volz KS, Tang Z, Red-Horse K and Ardehali R. Developmental heterogeneity of cardiac fibroblasts does not predict pathological proliferation and activation. Circ Res 2014;115:625–35. [PubMed: 25037571]

12. Zhou B, Honor LB, He H, Ma Q, Oh JH, Butterfield C, Lin RZ, Melero-Martin JM, Dolmatova E, Duffy HS, Gise A, Zhou P, Hu YW, Wang G, Zhang B, Wang L, Hall JL, Moses MA, McGowan FX and Pu WT. Adult mouse epicardium modulates myocardial injury by secreting paracrine factors. J Clin Invest 2011;121:1894–904. [PubMed: 21505261]

13. Trembley MA, Velasquez LS, de Mesy Bentley KL and Small EM. Myocardin-related transcription factors control the motility of epicardium-derived cells and the maturation of coronary vessels. Development 2015;142:21–30. [PubMed: 25516967]

14. Pipes GC, Creemers EE and Olson EN. The myocardin family of transcriptional coactivators: versatile regulators of cell growth, migration, and myogenesis. Genes Dev 2006;20:1545–56. [PubMed: 16778073]

15. Olson EN and Nordheim A. Linking actin dynamics and gene transcription to drive cellular motile functions. Nat Rev Mol Cell Biol 2010;11:353–65. [PubMed: 20414257]

16. Small EM. The actin-MRTF-SRF gene regulatory axis and myofibroblast differentiation. J Cardiovasc Transl Res 2012;5:794–804. [PubMed: 22898751]

17. Velasquez LS, Sutherland LB, Liu Z, Grinnell F, Kamm KE, Schneider JW, Olson EN and Small EM. Activation of MRTF-A-dependent gene expression with a small molecule promotes myofibroblast differentiation and wound healing. Proc Natl Acad Sci U S A 2013;110:16850–5. [PubMed: 24082095]

18. Yu-Wai-Man C, Spencer-Dene B, Lee RM, Hutchings K, Lisabeth EM, Treisman R, Bailly M, Larsen SD, Neubig RR and Khaw PT. Local delivery of novel MRTF/SRF inhibitors prevents scar tissue formation in a preclinical model of fibrosis. Sci Rep 2017;7:518. [PubMed: 28364121]

19. Shiwen X, Stratton R, Nikitorowicz-Buniak J, Ahmed-Abdi B, Ponticos M, Denton C, Abraham D, Takahashi A, Suki B, Layne MD, Lafyatis R and Smith BD. A Role of Myocardin Related Transcription Factor-A (MRTF-A) in Scleroderma Related Fibrosis. PLoS One 2015;10:e0126015. [PubMed: 25955164]

20. Zhou Y, Huang X, Hecker L, Kurundkar D, Kurundkar A, Liu H, Jin TH, Desai L, Bernard K and Thannickal VJ. Inhibition of mechanosensitive signaling in myofibroblasts ameliorates experimental pulmonary fibrosis. J Clin Invest 2013;123:1096–108. [PubMed: 23434591]

21. Small EM, Thatcher JE, Sutherland LB, Kinoshita H, Gerard RD, Richardson JA, Dimaio JM, Sadek H, Kuwahara K and Olson EN. Myocardin-related transcription factor-a controls myofibroblast activation and fibrosis in response to myocardial infarction. Circ Res 2010;107:294304.

22. Miano JM, Ramanan N, Georger MA, de Mesy Bentley KL, Emerson RL, Balza RO Jr., Xiao Q, Weiler H, Ginty DD and Misra RP. Restricted inactivation of serum response factor to the cardiovascular system. Proc Natl Acad Sci U S A 2004;101:17132–7. [PubMed: 15569937]

23. Jeong MY, Lin YH, Wennersten SA, Demos-Davies KM, Cavasin MA, Mahaffey JH, Monzani V, Saripalli C, Mascagni P, Reece TB, Ambardekar AV, Granzier HL, Dinarello CA and McKinsey TA. Histone deacetylase activity governs diastolic dysfunction through a nongenomic mechanism. Sci Transl Med 2018;10.

24. Fu X, Khalil H, Kanisicak O, Boyer JG, Vagnozzi RJ, Maliken BD, Sargent MA, Prasad V, Valiente-Alandi I, Blaxall BC and Molkentin JD. Specialized fibroblast differentiated states

underlie scar formation in the infarcted mouse heart. J Clin Invest 2018;128:2127–2143. [PubMed: 29664017]

25. Khalil H, Kanisicak O, Prasad V, Correll RN, Fu X, Schips T, Vagnozzi RJ, Liu R, Huynh T, Lee SJ, Karch J and Molkentin JD. Fibroblast-specific TGF-beta-Smad2/3 signaling underlies cardiac fibrosis. J Clin Invest 2017;127:3770–3783. [PubMed: 28891814]
26. Molkentin JD, Bugg D, Ghearing N, Dorn LE, Kim P, Sargent MA, Gunaje J, Otsu K and Davis J. Fibroblast-Specific Genetic Manipulation of p38 Mitogen-Activated Protein Kinase In Vivo Reveals Its Central Regulatory Role in Fibrosis. Circulation 2017;136:549–561. [PubMed: 28356446]
27. Long MA and Rossi FM. Silencing inhibits Cre-mediated recombination of the Z/AP and Z/EG reporters in adult cells. PLoS One 2009;4:e5435. [PubMed: 19415111]
28. Schmidt-Supprian M and Rajewsky K. Vagaries of conditional gene targeting. Nat Immunol 2007;8:665–8. [PubMed: 17579640]
29. Kanisicak O, Khalil H, Ivey MJ, Karch J, Maliken BD, Correll RN, Brody MJ, SC JL, Aronow BJ, Tallquist MD and Molkentin JD. Genetic lineage tracing defines myofibroblast origin and function in the injured heart. Nat Commun 2016;7:12260. [PubMed: 27447449]
30. Sharma B, Ho L, Ford GH, Chen HI, Goldstone AB, Woo YJ, Quertermous T, Reversade B and Red-Horse K. Alternative Progenitor Cells Compensate to Rebuild the Coronary Vasculature in Elabela- and Apj-Deficient Hearts. Dev Cell 2017;42:655–666 e3. [PubMed: 28890073]
31. He L, Li Y, Li Y, Pu W, Huang X, Tian X, Wang Y, Zhang H, Liu Q, Zhang L, Zhao H, Tang J, Ji H, Cai D, Han Z, Han Z, Nie Y, Hu S, Wang QD, Sun R, Fei J, Wang F, Chen T, Yan Y, Huang H, Pu WT and Zhou B. Enhancing the precision of genetic lineage tracing using dual recombinases. Nat Med 2017;23:1488–1498. [PubMed: 29131159]
32. Alva JA, Zovein AC, Monvoisin A, Murphy T, Salazar A, Harvey NL, Carmeliet P and Iruela-Arispe ML. VE-Cadherin-Cre-recombinase transgenic mouse: a tool for lineage analysis and gene deletion in endothelial cells. Dev Dyn 2006;235:759–67. [PubMed: 16450386]
33. Kisanuki YY, Hammer RE, Miyazaki J, Williams SC, Richardson JA and Yanagisawa M. Tie2-Cre transgenic mice: a new model for endothelial cell-lineage analysis in vivo. Dev Biol 2001;230:230–42. [PubMed: 11161575]
34. Clausen BE, Burkhardt C, Reith W, Renkawitz R and Forster I. Conditional gene targeting in macrophages and granulocytes using LysMcre mice. Transgenic Res 1999;8:265–77. [PubMed: 10621974]
35. Stadtfeld M and Graf T. Assessing the role of hematopoietic plasticity for endothelial and hepatocyte development by non-invasive lineage tracing. Development 2005;132:203–13. [PubMed: 15576407]
36. Wirth A, Benyo Z, Lukasova M, Leutgeb B, Wettschureck N, Gorbey S, Orsy P, Horvath B, Maser-Gluth C, Greiner E, Lemmer B, Schutz G, Gutkind JS and Offermanns S. G12-G13LARG-mediated signaling in vascular smooth muscle is required for salt-induced hypertension. Nat Med 2008;14:64–8. [PubMed: 18084302]
37. Zhu X, Hill RA, Dietrich D, Komitova M, Suzuki R and Nishiyama A. Age-dependent fate and lineage restriction of single NG2 cells. Development 2011;138:745–53. [PubMed: 21266410]
38. Cai CL, Martin JC, Sun Y, Cui L, Wang L, Ouyang K, Yang L, Bu L, Liang X, Zhang X, Stallcup WB, Denton CP, McCulloch A, Chen J and Evans SM. A myocardial lineage derives from Tbx18 epicardial cells. Nature 2008;454:104–8. [PubMed: 18480752]
39. Acharya A, Baek ST, Banfi S, Eskiocak B and Tallquist MD. Efficient inducible Cremediated recombination in Tcf21 cell lineages in the heart and kidney. Genesis 2011;49:870–7. [PubMed: 21432986]
40. Porrello ER, Mahmoud AI, Simpson E, Hill JA, Richardson JA, Olson EN and Sadek HA. Transient regenerative potential of the neonatal mouse heart. Science 2011;331:1078–80. [PubMed: 21350179]
41. Lepilina A, Coon AN, Kikuchi K, Holdway JE, Roberts RW, Burns CG and Poss KD. A dynamic epicardial injury response supports progenitor cell activity during zebrafish heart regeneration. Cell 2006;127:607–19. [PubMed: 17081981]

42. Wei K, Serpooshan V, Hurtado C, Diez-Cunado M, Zhao M, Maruyama S, Zhu W, Fajardo G, Noseda M, Nakamura K, Tian X, Liu Q, Wang A, Matsuura Y, Bushway P, Cai W, Savchenko A, Mahmoudi M, Schneider MD, van den Hoff MJ, Butte MJ, Yang PC, Walsh K, Zhou B, Bernstein D, Mercola M and Ruiz-Lozano P. Epicardial FSTL1 reconstitution regenerates the adult mammalian heart. Nature 2015;525:479–85. [PubMed: 26375005]

43. Biernacka A and Frangogiannis NG. Aging and Cardiac Fibrosis. Aging Dis 2011;2:158173.

44. Sisson TH, Ajayi IO, Subbotina N, Dodi AE, Rodansky ES, Chibucos LN, Kim KK, Keshamouni VG, White ES, Zhou Y, Higgins PD, Larsen SD, Neubig RR and Horowitz JC. Inhibition of myocardin-related transcription factor/serum response factor signaling decreases lung fibrosis and promotes mesenchymal cell apoptosis. Am J Pathol 2015;185:969–86. [PubMed: 25681733]

45. Trembley MA, Quijada P, Agullo-Pascual E, Tylock KM, Colpan M, Dirkx RA Jr., Myers JR, Mickelsen DM, de Mesy Bentley K, Rothenberg E, Moravec CS, Alexis JD, Gregorio CC, Dirksen RT, Delmar M and Small EM. Mechanosensitive Gene Regulation by Myocardin-Related Transcription Factors Is Required for Cardiomyocyte Integrity in Load-Induced Ventricular Hypertrophy. Circulation 2018;138:1864–1878. [PubMed: 29716942]

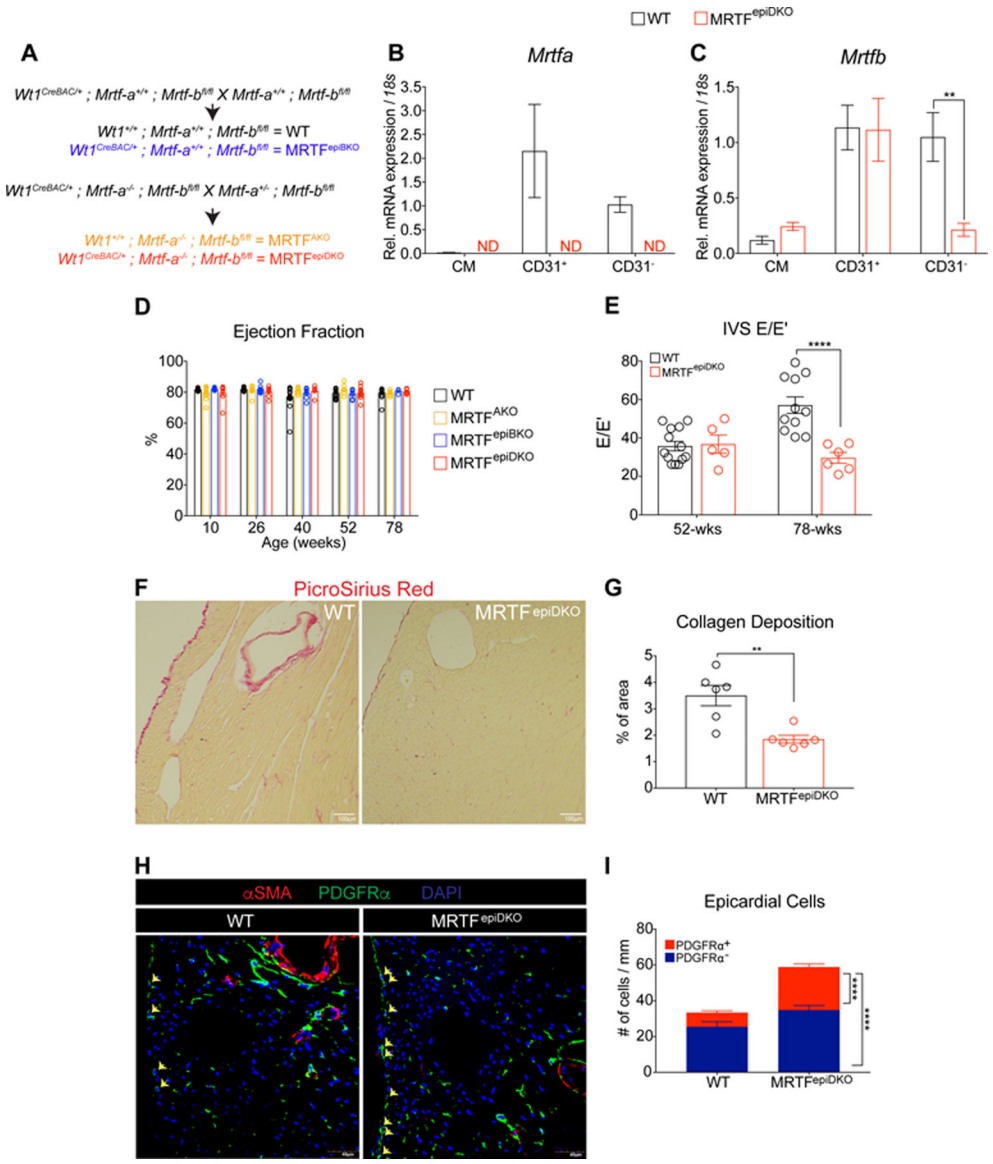

Figure 1. Aged-associated diastolic dysfunction is prevented in MRTF^{epiDKO} mice.

(A) Breeding strategy for the generation of WT and MRTF transgenic mice. **(B)** *Mrtfa* and (**C**) *Mrtfb* expression in CMs, CD31^{+} and CD31^{-} cell populations isolated from WT and MRTF^{epiDKO} hearts. ND = Not Detected. **(D)** Ejection Fraction (%) measured in female WT and MRTF transgenic mice during aging. **(E)** E to E prime ratio (Interventricular Septum or IVS E/E') measured by tissue doppler at 52 and 78-weeks of age. **(F)** Representative staining of collagen by Picro Sirius Red staining at 78-weeks of age. **(G)** Quantitation of collagen visualized in the left ventricle of the heart (% of area). **(H)** Representative images of PDGFRα^{-} and PDGFRα^{+} epicardial cells represented as DAPI^{+} nuclei outside the myocardial border (yellow arrows). **(I)** Quantitation of PDGFRα^{-} and PDGFRα^{+} epicardial cells at 78-weeks of age.

Scale bar **(F)** = 100μm. Scale bar **(H)** = 40μm.

** p<0.01, **** p<0.0001.

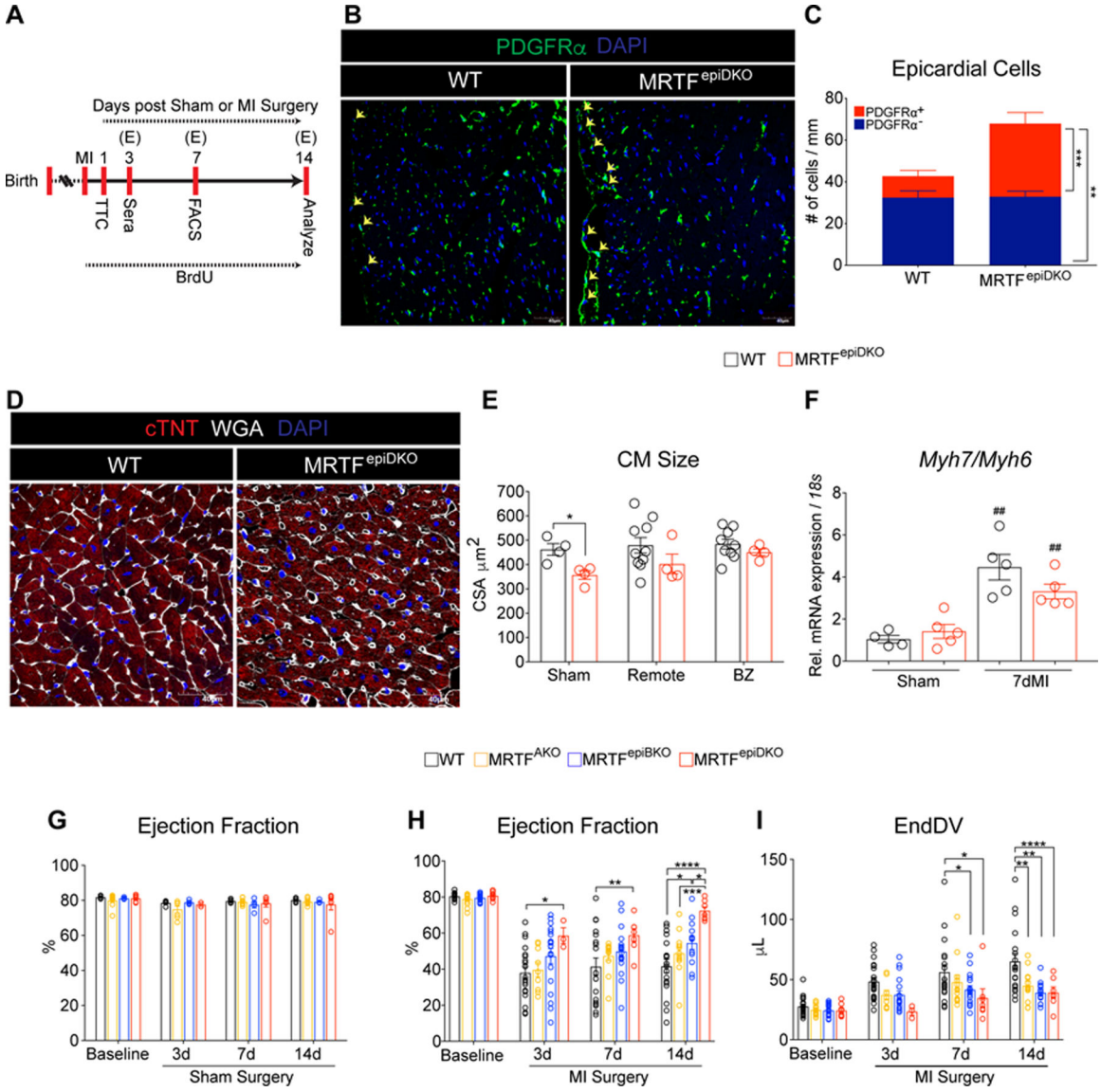

Figure 2. Preservation of cardiac physiology in MRTF^{epiDKO} hearts after MI.

(A) Time-line analysis of adult male WT and MRTF transgenic mice subjected to Sham or MI surgery at 10–12 weeks of age. MRTF transgenic mice were analyzed by echocardiography (E) prior to surgery (baseline) and 3, 7 and 14 days after surgery. **(B)** Representative images of PDGFRα^{-} and PDGFRα^{+} epicardial cells represented as DAPI^{+} nuclei outside the myocardial border (yellow arrows). **(C)** Quantitation of PDGFRα^{-} and PDGFRα^{+} epicardial cells in 12-week old sham mice. **(D)** CM size was visualized in young (12-week old) sham mice. **(E)** Quantitation of CM crosssectional area (CSA; μm^2) in sham and injured mice. **(F)** CM fetal gene expression of *Myh7/Myh6*. **(G)** Ejection Fraction (%) measured in male WT and MRTF transgenic mice following sham surgery. **(H)** Ejection fraction (%) and **(I)** End Diastolic Volume (μL) measurements following MI surgery. Scale bar **(B and D)** = 40μm.

* p<0.05, ** p<0.01, *** p<0.001, **** p<0.0001.

p<0.01: 7dMI versus Sham.

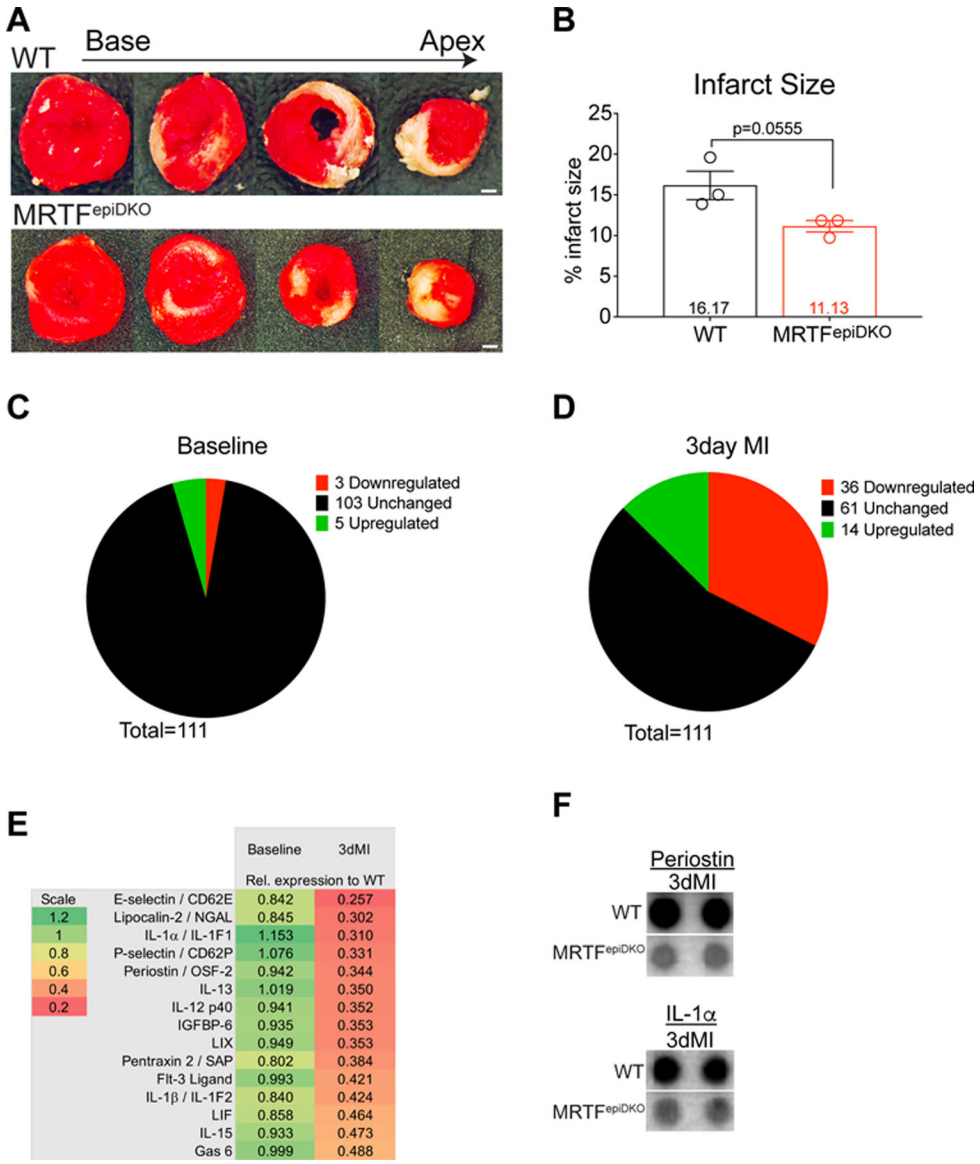

Figure 3. MRTF^{epiDKO} mice are protected from pathological fibrotic remodeling following MI.

(A) Representative WT and MRTF^{epiDKO} heart sections stained with TTC and quantitated in **(B)** 24 hours post-MI. 111 cytokines were measured and categorized as unchanged (black), upregulated (green) or downregulated (red). Screen was performed in **(C)** Non-injured mice and **(D)** Mice subjected to MI for 3-days. **(E)** List of downregulated cytokines in MRTF^{epiDKO} serum relative to WT serum at baseline and 3-days post-MI. Representative dot blot images of **(F)** Periostin and IL-1α / IL-1F1 at 3-days post MI.

Scale bar **(A)** = 1mm.

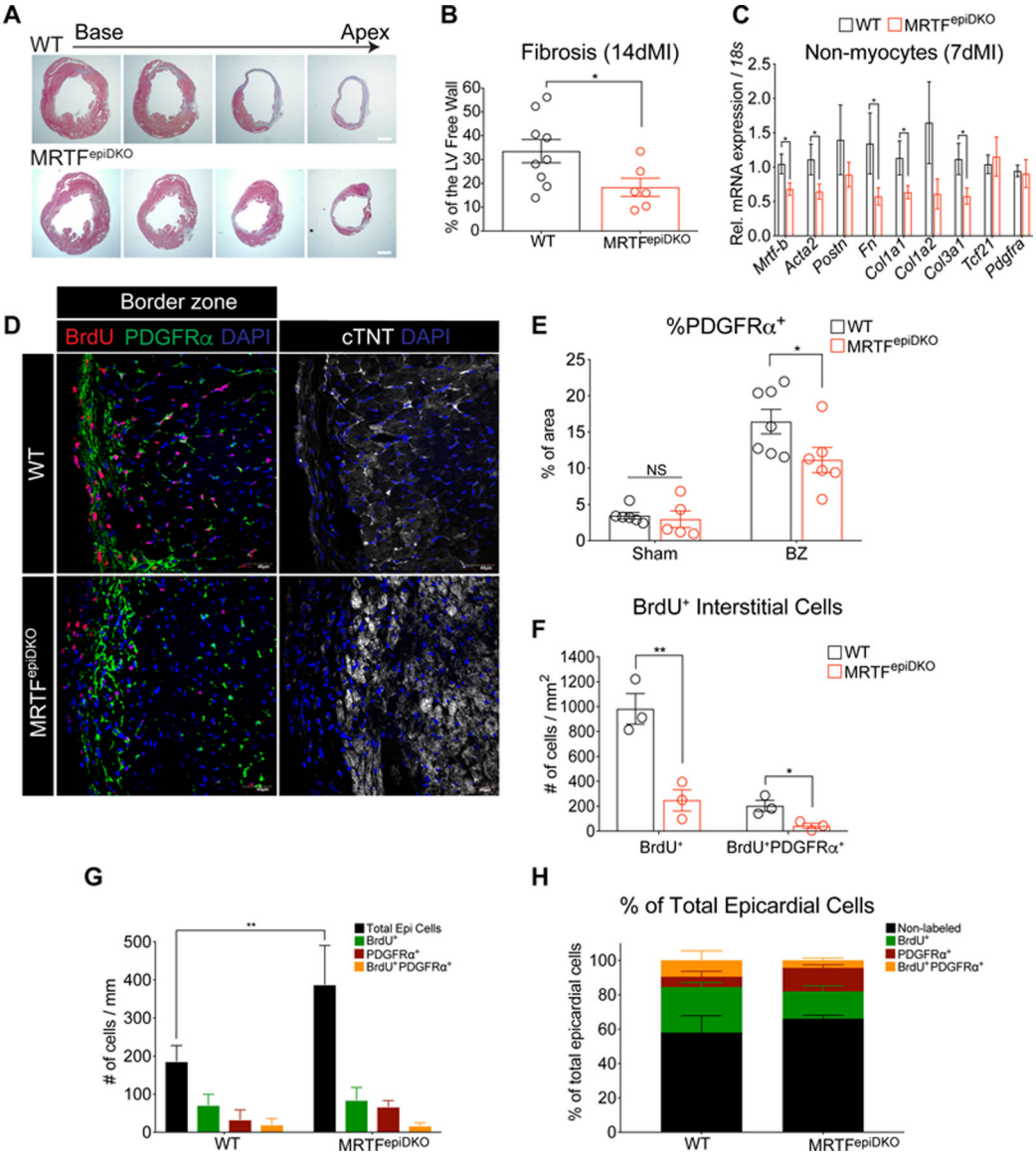

Figure 4. Cardiac fibrosis is attenuated in MRTF^{epiDKO} hearts after MI.

(A) WT and MRTF^{epiDKO} hearts represented in 4 layers after staining with Masson's Trichrome. **(B)** Quantitation of left ventricular free wall fibrosis (%) 14 days after MI. **(C)** Gene expression in nonmyocytes isolated from female WT and MRTF^{epiDKO} adult hearts 7-days post-MI. **(D)** Visualization of PDGFRα^{-} and PDGFRα^{+} epicardial cells represented as DAPI^{+} nuclei outside the myocardial border and labeling of BrdU^{+} cells in the epicardium and interstitium in the BZ regions of the heart 14 days post-MI. **(E)** Quantitation of PDGFRa protein expression (% of area) located in sham and BZ regions of the heart 14 days post-injury. **(F)** Quantitation of the number of BrdU^{+} interstitial cells in the BZ regions of WT and MRTF^{epiDKO} hearts. **(G)** Quantitation of epicardial cells, BrdU^{+}, PDGFRα$^{+\cdot}$, and BrdU^{+}/PDGFRα^{+} epicardial cells in BZ regions of the heart. **(H)** Fraction of total epicardial cells (normalized to 100%) categorized as non-labeled, BrdU^{+}, PDGFRα^{+}, and BrdU^{+}/PDGFRα^{+} in the BZ regions of the heart.

Scale bar **(A)** = 1mm. Scale bar **(D)** = 40μm.
* $p<0.05$, ** $p<0.01$.

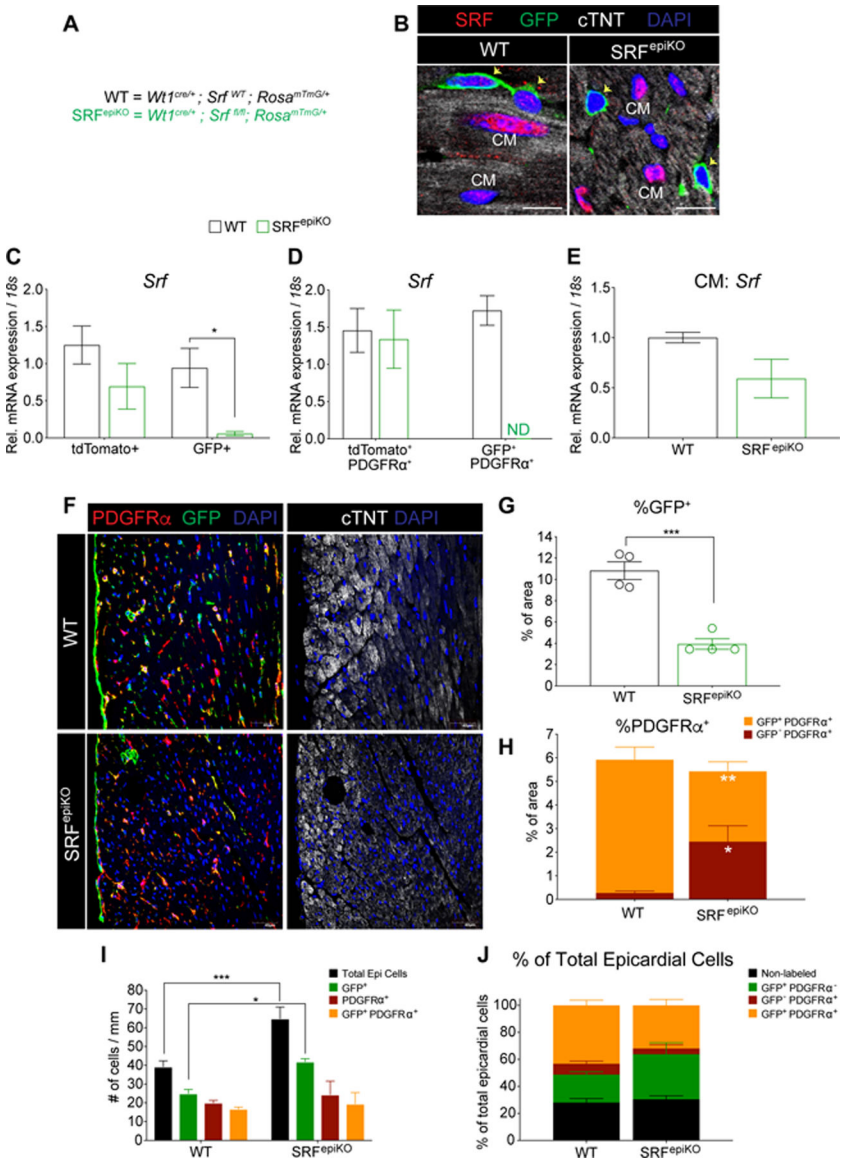

Figure 5. SRF is required for EPDC investment of the adult cardiac interstitium.

(A) Breeding strategy for the generation of WT and SRF transgenic mice. **(B)** SRF protein detected in *Wt1* lineage-derived cells (GFP$^+$ = green) and CMs from WT and SRF^{epiKO} hearts. *Srf* expression in **(C)** tdTomato$^+$ and GFP$^+$ cells, **(D)** tdTomato$^+$ PDGFRα$^+$ and GFP$^+$ PDGFRα$^+$ cells and **(E)** CMs isolated from sham-operated animals. **(F)** Representative images of *Wt1* lineage-derived cells (GFP$^+$) and PDGFRα$^+$ cells in the epicardium and interstitial areas. Epicardial cells are represented as DAPI$^+$ nuclei outside the myocardial border in WT and SRF^{epiKO} mice. **(G)** Quantitation of GFP protein expression (% of area). **(H)** Distribution of GFP$^-$/PDGFRα and GFP$^+$/PDGRa$^+$ protein expression. **(I)** Quantitation of GFP$^+$, PDGFRα$^+$, and GFP$^+$/PDGFRα$^+$ epicardial cells. **(J)** Fraction of total epicardial cells (normalized to 100%) categorized as nonlabeled, GFP$^+$, PDGFRα$^+$, or GFP$^+$/PDGFRα$^+$.

Scale bar **(B)** = 10μm. Scale bar **(F)** = 40μm.

* p<0.05, ** p<0.01, *** p<0.001, ****p<0.0001.

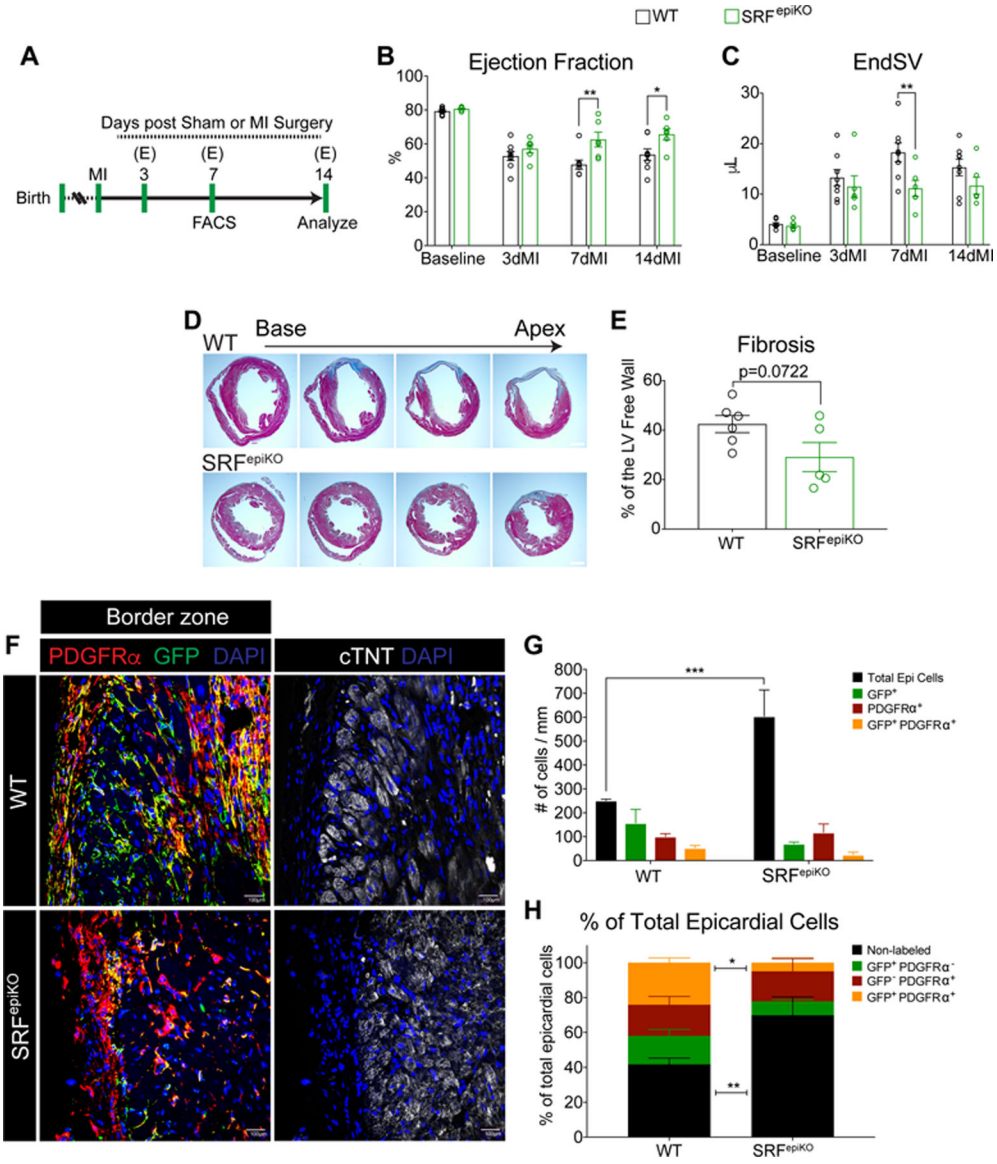

Figure 6. SRF^{epiKO} mice show modest preservation of cardiac function and exaggerated epicardial activation in response to MI.

(A) Time-line analysis of adult WT and SRF^{epiKO} mice subjected to MI. Echocardiography (E) was conducted prior to surgery and 3, 7 and 14 days after surgery. **(B)** Ejection fraction (%) and **(C)** End Systolic Volume (μL) in WT and SRF^{epiKO} mice. **(D)** WT and SRF^{epiKO} hearts represented in 4 layers to visualize cardiac fibrosis (Masson's Trichrome stain). **(E)** Quantitation of left ventricular free wall fibrosis (%) after MI. **(F)** Visualization of epicardial cells labeled for GFP and/or PDGFRα represented as DAPI^{+} nuclei outside the myocardial border in the BZ regions of the heart 14 days post-MI. **(G)** Quantitation of total epicardial cells, GFP^{+}, PDGFRα^{+}, and GFP^{+}/PDGFRα^{+} epicardial cells in BZ regions of the heart. **(H)** Fraction of total epicardial cells (normalized to 100%) categorized as non-labeled, GFP^{+}, PDGFRα^{+}, or GFP^{+}/PDGFRα^{+} in the BZ regions of the heart.

Scale bar **(D)** = 1mm. Scale bar **(F)** = 40μm.

* p<0.05, ** p<0.01, *** p<0.001.

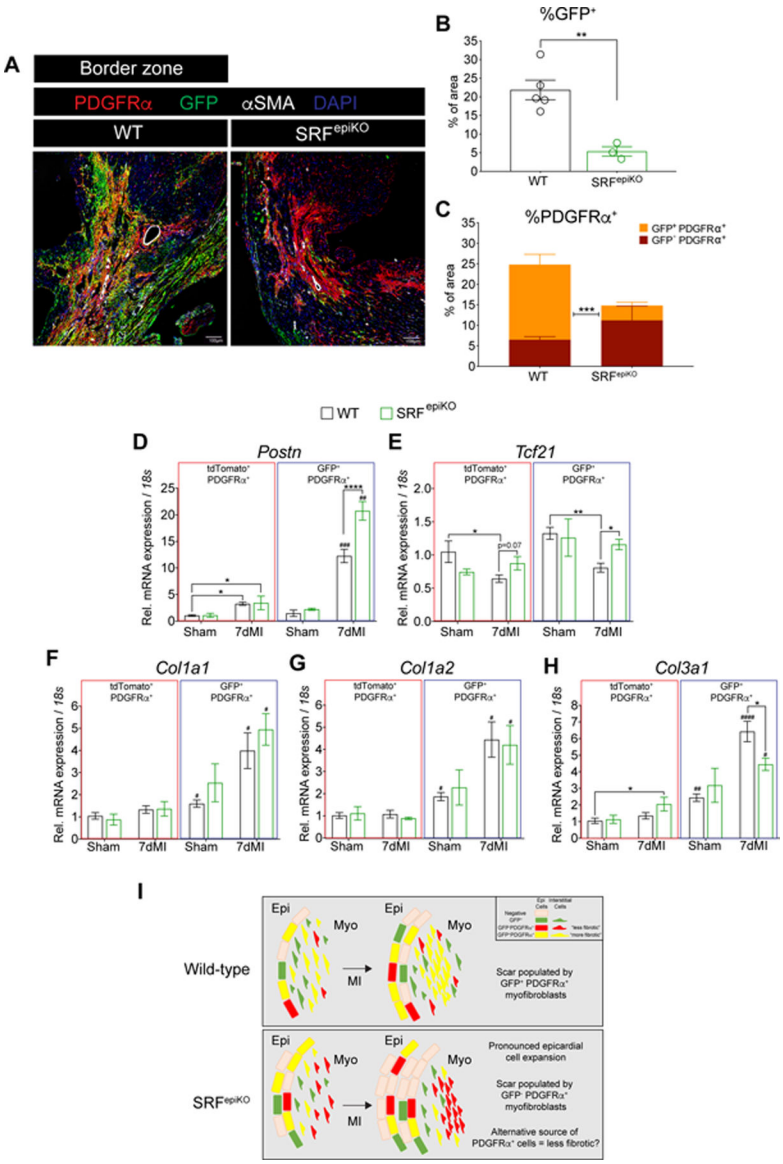

Figure 7. Infarct re-cellularization requires SRF expression in EPDCs.

(A) Labeling of *Wt1* lineage derived cells (GFP^{+}) and PDGFRα^{+} cells in WT and SRF^{epiKO} mice. **(B)** Quantitation of GFP protein expression in the BZ regions and 14 days post MI (% of area). **(C)** Distribution of GFP^{-}/PDGFRα^{+} and GFP^{+}/PDGRα^{+} protein expression. Gene expression analysis of GFP^{+}/PDGFRα^{+} and tdTomato^{+}/PDGFRα^{+} cells isolated by FACS from sham surgical mice and mice subjected to MI for 7 days. **(D)** *Postn*, **(E)** *Tcf21*, **(F)** *Col1a1*, **(G)** *Col1a2*, and **(H)** *Col3a1*. **(I)** Schematic of proposed cellular mechanism of epicardial-derived fibrosis in the adult heart after MI. In non-injured conditions, WT mice show maintenance of epicardial-derived PDGFRα^{+} myofibroblasts, which expand in response to MI. In contrast, SRF^{epiKO} mice show reduced investment of epicardial-derived PDGFRα^{+} cells at baseline and following MI. Alternative to the response in WT mice, the scar is re-populated with GFP^{-}PDGFRα^{+} myofibroblasts, a nonepicardial cell lineage that is

likely descended from an alternative “less fibrotic” cell lineage. EPI = epicardium. MYO = myocardium. MI = Myocardial Infarction.

Scale bar **(A)** = 40μm.

* p<0.05, ** p<0.01, ****p<0.0001.

# p<0.05, ## p<0.01, ### p<0.001, #### p<0.0001: GFP^+/$PDGFR\alpha^+$ versus $tdTomato^+$/$PDGFR\alpha^+$.